



ELSEVIER

Contents lists available at ScienceDirect

## Deep-Sea Research I

journal homepage: [www.elsevier.com/locate/dsrI](http://www.elsevier.com/locate/dsrI)

## Dispersion of a tracer on the East Pacific Rise (9°N to 10°N), including the influence of hydrothermal plumes

P.R. Jackson<sup>a,1</sup>, J.R. Ledwell<sup>b,\*</sup>, A.M. Thurnherr<sup>c,2</sup>

<sup>a</sup> United States Geological Survey, Illinois Water Science Center, 1201 W. University Ave., Suite 100, Urbana, IL 61801, USA

<sup>b</sup> Applied Ocean Physics and Engineering Department, Woods Hole Oceanographic Institution, Woods Hole, MA 02543, USA

<sup>c</sup> Lamont-Doherty Earth Observatory, Columbia University, USA

## ARTICLE INFO

## Article history:

Received 19 November 2008

Received in revised form

12 August 2009

Accepted 30 October 2009

## Keywords:

Ocean mixing

East Pacific Rise

Hydrothermal vent plume

Tracer experiment

Larval transport

## ABSTRACT

On 12 November 2006, 3 kg of sulfur hexafluoride were released in a 1.2 km long streak in the axial summit trough of the East Pacific Rise at 9°30'N to study how circulation and mixing affect larval dispersion. The first half of a tracer survey performed approximately 40 days after the injection found a small percentage of the tracer on the ridge axis between 9°30'N and 10°10'N, with the main concentration near 9°50'N, a site of many active hydrothermal vents. These observations provide evidence of larval connectivity between vent sites on the ridge. The latter half of the survey detected the primary patch of tracer west of the ridge and just south of the Lamont Seamounts, as a majority of the tracer had been transported off the ridge. However, by the end of the survey, the eastern edge of this patch was transported back to within 10 km of the ridge crest at 9°50'N by a reversal in the subinertial flow, suggesting another pathway for larvae between points along the ridge. Both the horizontal and vertical distributions of the tracer were complex and were likely heavily influenced by topography and vents in the area. Elevated tracer concentrations within the axial summit trough and an adjacent depression on the upper ridge flank suggest that tracers may be detained in such depressions. Correlated tracer/turbidity profiles provide direct evidence of entrainment of the tracer into vent plumes from 9°30'N to 10°N. A comparison of the vertical tracer inventory with neutral density vent-plume observations suggests that on the order of 10% of the tracer injected was entrained into vent plumes near the injection site. The results imply that effluent from diffuse hydrothermal sources and larvae of hydrothermal vent fauna can be entrained in significant quantities into plumes from discrete sources and dispersed in the neutrally buoyant plumes.

© 2009 Elsevier Ltd. All rights reserved.

### 1. Introduction

Hydrothermally active mid-ocean ridges are known for their complex topography and flows. The dispersal pathways for chemical species and plankton originating on the ridge crest involve topographically induced flows and hydrothermal vent plumes, as well as the full spectrum of motions generally prevalent in the ocean. Tracking the dispersion of many natural tracers (chemical or biological) is complicated by the temporal variability in the sources and regional hydrography and circulation and the difficulty in connecting a source with the dispersed scalar (numerous sources typically exist on a ridge segment). Further complications arise from the non-conservative nature of some natural tracers.

Here we describe the release of a conservative tracer within the axial summit trough (AST) of the East Pacific Rise, and its subsequent dispersion. Our primary objective was to mimic the dispersion of planktonic larvae of vent species. The time scale of the experiment was set by the average life span of *Riftia pachyptila* larvae (38 days, Marsh et al., 2001). The final distribution of the tracer suggests pathways to other parts of the ridge by topographically induced flows and by mesoscale variability. The distribution of the tracer in density space gives an estimate of the diapycnal diffusivity for the general area at and around the ridge crest. Some of the tracer, however, was clearly entrained into hydrothermal vent plumes, and the fraction of tracer found in the density range of the neutrally buoyant plumes provides an estimate of the probability of entrainment for a passive tracer released at our site.

The paper is organized as follows. The tracer injection in the AST at 9°30'N is described in Section 2, along with some measurements of the currents near the injection site. The lateral and vertical distributions of the tracer, sampled several weeks after the injection, are presented in Section 3. A presentation of

\* Corresponding author. Tel.: +1 508 289 3305; fax: +1 508 457 2194.

E-mail addresses: [pjackson@usgs.gov](mailto:pjackson@usgs.gov) (P.R. Jackson), [jledwell@whoi.edu](mailto:jledwell@whoi.edu) (J.R. Ledwell), [ant@ldeo.columbia.edu](mailto:ant@ldeo.columbia.edu) (A.M. Thurnherr).

<sup>1</sup> Tel.: +1 217 328 9719; fax: +1 217 344 0082.

<sup>2</sup> Tel.: +1 845 365 8816; fax: +1 845 365 8157.

our vent-plume observations in Section 4 sets the stage for a quantitative estimate of tracer entrainment into these plumes in Section 5. In Section 6 we discuss several topics: our scenario for the flow pattern that brought the tracer to its final distribution; evidence for sheltering of tracer in the axial summit trough and other depressions; contributions of diffuse sources to the neutrally buoyant plumes at this ridge segment; and how all of these relate to the dispersal of planktonic vent larvae.

## 2. Tracer injection

### 2.1. The site

The tracer release experiment took place on the fast spreading East Pacific Rise (EPR) between 9°N and 10°N in late 2006 during the first two legs of a field program, dubbed LADDER, an acronym derived from the goal to study Larval Dispersal along the Deep East Pacific Rise (Fig. 1; we refer to the two cruises discussed in this paper as LADDER 1 and LADDER 2). This segment of the EPR has a strike of 352° (Macdonald et al., 1992), and is bounded by the Clipperton and Siqueiros transform faults in the north and south, respectively. The ridge is relatively uniform in cross section between 9°10'N and 10°N, rising steeply (slope ~0.04) from about 3000 m on the less steep (slope ~0.003) outer ridge flanks to about 2500 m depth along the summit. Paralleling the ridge on both flanks are bathymetric hills (or fault scarps), forming ridges with vertical scales between 25 and 100 m and typical horizontal

spacing of 2.5–5 km. South of 9°10'N, there is a discontinuity in the ridge axis known as the 9°03'N overlapping spreading center (OSC). The Lamont seamount chain lies to the west of the ridge near 9°50'N and consists of five or six seamounts, the highest of which rises nearly 1000 m above the EPR crest, to 1648 m, making these seamounts the shallowest topographic features in the area.

Along the crest of the EPR runs the AST, a shallow (< 15 m deep) and narrow (40–200 m wide, Fornari et al., 1998) depression, with interruptions that can span 5 km or more. While hydrothermal activity is found along the entire ridge segment, primarily within the AST, many studies have focused on the 9°50'N area which has been designated as the “Bull’s Eye” for this Integrated Study Site (ISS) by the Ridge 2000 program. Fig. 1 shows the locations of known high-temperature vents within the study area (vent locations may be found at <http://marine-geo.org/tools/search/targets.php?id=EPR>). Low temperature diffuse sources are less well documented, but they are numerous, span large areas, and can produce a considerable amount of hydrothermal fluid (Rona and Trivett, 1992; Baker et al., 1993; Lavelle and Wetzler, 1999; Lavelle et al., 2001). Although many diffuse flow sites are in close proximity to high temperature vents, isolated diffuse sources also exist along the EPR.

The local currents on the ridge crest near 9°50'N have been measured in the context of several different studies with the intent of understanding the dynamics of larval transport (Chevaldonné et al., 1997; Marsh et al., 2001; Mullineaux et al., 2002; Adams and Mullineaux, 2008). At the broadest scale, there is a westward drift that has been shown to advect hydrothermal plumes thousands of kilometers to the west into the interior of the North Pacific (Craig, 1990; Talley and Johnson, 1994; Lupton, 1998). Measurements on the ridge crest have shown subinertial flows that are predominately along-ridge but that reverse direction on time scales of 3 weeks to 2 months (Marsh et al., 2001; Chevaldonné et al., 1997; Adams, 2007). Preliminary results from a 2-D numerical model of the EPR (W.J. Lavelle, personal communication) and field measurements (e.g., Adams, 2007) show that subinertial currents along the upper flanks of the EPR are oriented to the south on the eastern side of the ridge and to the north on the western side of the ridge. In the 2-D model these upper flank currents arise from rectification, in a general sense, of cross-ridge oscillatory flows. The flow within the AST on the EPR may be oriented along the strike of the axis due to steering of the flow by the topography, though no measurements have been made within the relatively shallow trough of the EPR to verify this.

### 2.2. The tracer injection system

The tracer injection system used in this study was an *Alvin*-compatible version of the system described by Watson and Ledwell (2000). It consisted of a control module inside *Alvin*'s sphere and the pump, electronics, and distribution system mounted on *Alvin*'s bow basket. The control module allowed the user to regulate the flow of SF<sub>6</sub> and the fluid used to prime the pump and test the system at low external pressure. The primer fluid was changed for this experiment from 2-propanol, used in the past, to 2,3-dihydroperfluoropentane for better compatibility with SF<sub>6</sub>. The tracer and primer fluids were contained in two separate accumulators mounted aft on the basket. The distribution system consisted of a four-port manifold with individual valves and 50-μm ceramic orifices for each port mounted on an arm 56 cm above the basket and oriented about 10° aft, off the starboard side of the submersible. Each valve was fitted with a T-bar handle to fit *Alvin*'s manipulators. A pressure gauge on the manifold allowed the operator to monitor the overpressure across

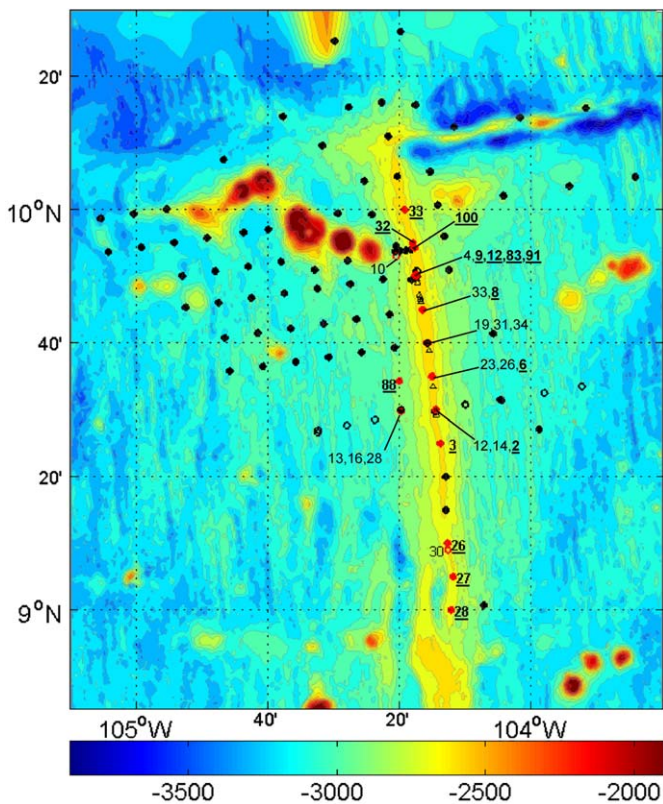


Fig. 1. Study site along the northern East Pacific Rise. Dots show CTD/LADCP stations (open circles, LADDER 1; closed circles, LADDER 2). Black triangles show locations of known high temperature hydrothermal vents. Casts in which a neutrally buoyant hydrothermal plume was detected are shown in red and labeled with the cast number for that cruise (normal, LADDER 1; underlined, LADDER 2). The bathymetry is from a SeaBeam survey (Macdonald et al., 1992) with gaps filled with altimetry (Smith and Sandwell, 1997). The tracer was released along the ridge at 9°30'N, where casts 12, 14, and 2 are located.

the orifice. Multiple injection ports provided redundancy, as past injections with similar systems had repeated problems with clogging of the orifice, primarily when switching from primer fluid to tracer. The new primer fluid seems to have greatly reduced this problem, as only the first orifice was needed for the injection.

### 2.3. Tracer injection

Three kilograms of SF<sub>6</sub> were injected in a 1200 m long streak within the AST at 9°30'N on the EPR on 12 November 2006 during *Alvin* dive 4271. The tracer was released at a steady rate of 15 ml/min (20 g/min) over 2.5 h with *Alvin* moving from north to south at an average speed of 0.13 m/s. The injection orifices were 0.50 m above the face of the transponder on the Benthos altimeter on *Alvin*. The mean height of the orifice above the bottom during injection was 4.8 m, with a standard deviation of 1.8 m, due largely to the rough topography of the trough.

The bathymetry of the injection region had been surveyed on *Alvin* dive 4259. The AST over the injection reach had an average width of 160 m and an average depth of 9 m. The eastern wall of the trough was about 11 m high on average and relatively steep and well defined, while the western wall was of a variable height (10 m tall and steep to the south, tiered with roughly 6 and 4 m tiers to the north). Bottom topography within the AST varied dramatically, from tall pillars in the north to relatively smooth pillow lava and deep fissures in the south. Inactive sulfide structures had formed mounds or sills within the AST, forcing the submarine to maneuver around or over these obstructions. Hollow pillow lava, collapse pits, and fissures provided numerous pockets where tracer might be trapped.

Visual observations of injection of SF<sub>6</sub> into the ocean were made for the first time in this experiment. SF<sub>6</sub> forms a clathrate with pure water at the temperature and pressure of the injection (Sortland and Robinson, 1964). The milky color of the jet emitted from the orifice (Fig. 2) was most likely due to the formation of such a clathrate with seawater. The liquid SF<sub>6</sub> emerges from the orifice as droplets less than 100 μm in diameter (Watson and Ledwell, 2000). Upon contact with the water, these droplets most likely fragment into clathrate flakes within a second or so, the time scale for water to diffuse into the droplets. The molecular ratio of H<sub>2</sub>O to SF<sub>6</sub> in the clathrate is 17:1, and so the density anomaly of the particles is much less than that of liquid SF<sub>6</sub>. Immediately after forming, the flakes begin to dissolve as they fall through the ambient water. Simple estimates based on diffusion limited dissolution from a particle falling at Stokes fall velocity (Watson et al., 1987) suggest that the flakes dissolve before falling a few cm. Hence, the tracer should have dissolved by the time it



Fig. 2. A jet of SF<sub>6</sub> tracer issuing from a 50-μm orifice.

reached the back of the submarine. This scenario is consistent with observations of the visible tracer plume disappearing within several meters of the injection orifice, at which point the plume was about 20–30 cm wide. The tracer then traveled along the body of the submarine (and perhaps within the body panels) and was then caught in the submarine's turbulent wake. Further analysis of this mixing is given in the next section and in Appendix A.

A SeaBird SBE 19 CTD oriented fore/aft on *Alvin*'s basket measured conductivity, temperature, and pressure at 1 Hz during the injection to estimate variations in the density of water tagged by the tracer (Fig. 3; Statistics are given in Table 1). The time constant of the temperature sensor on this instrument was about 0.7 s, and that of the unpumped conductivity cell at the vehicle speed of 0.13 m s<sup>-1</sup> was about the same. The vertical temperature gradient is four times more important than the vertical salinity gradient in governing the vertical density gradient in the vicinity of the ridge crest. Yet, the high frequency density variations seen in Fig. 3 are almost entirely due to apparent salinity variations. We conclude that these salinity variations are mostly artificial, caused by the lag between the conductivity cell and the temperature sensor.

Temperature variations in the CTD record during the injection were dominated by short duration positive excursions as great as 0.02 °C above a generally quiet baseline (Fig. 3). We attribute these excursions to the proximity of diffuse sources of heated water from the seabed. We do not know the corresponding excursions in salinity, or indeed other variations in the composition of this warm water, and so variations in density due to variations in salinity or composition are unknown. That said, the root mean square (rms) temperature variation of 0.002 °C would by itself give an rms density variation of  $3.0 \times 10^{-4}$  kg/m<sup>3</sup> if the salinity were constant. This density variation corresponds to a depth variation of about 20 m in the vicinity of the ridge crest outside of the rather well mixed layer within and right above the AST.

### 2.4. Estimate of the initial plume

We estimate in Appendix A that the tracer more or less filled the AST along the injection reach within 4 or 5 h after the passage of the submarine (Fig. 4). In some locations where the trough is shallow and the submarine maintained an above-average altitude, tracer may have been able to escape the AST to the west during this time. The average tracer concentration in the AST shortly after injection, and before very much escaped, would have been on the order of 10 nmol/kg, based on the dimensions of the AST. This concentration is far too small to have significantly affected the density of the seawater.

The spread of densities occupied by the tracer shortly after injection is important to estimates of diapycnal mixing and plume entrainment. CTD casts into the AST between 9°05'N and 9°55'N during the deployment cruise (LADDER 1; 24 October to 18 November 2006) found either buoyant plumes in the bottom 40 m (5 casts) or vertical potential density gradients (9 casts) with absolute values of less than  $3 \times 10^{-6}$  kg/m<sup>4</sup>. This value is about five times smaller than the density gradient in the same density class on the flanks of the ridge. The CTD on *Alvin* found similarly weak stratification as it rose out of the AST at the end of each dive. As noted above, we estimate that most of the tracer was initially confined to the AST, which was only 9 m deep, on average. So, aside from transport in vent plumes to be discussed later, the range of densities occupied by the tracer at a given point along the injection reach was less than  $3 \times 10^{-5}$  kg/m<sup>3</sup>. This range is small compared with the rms density variations associated with

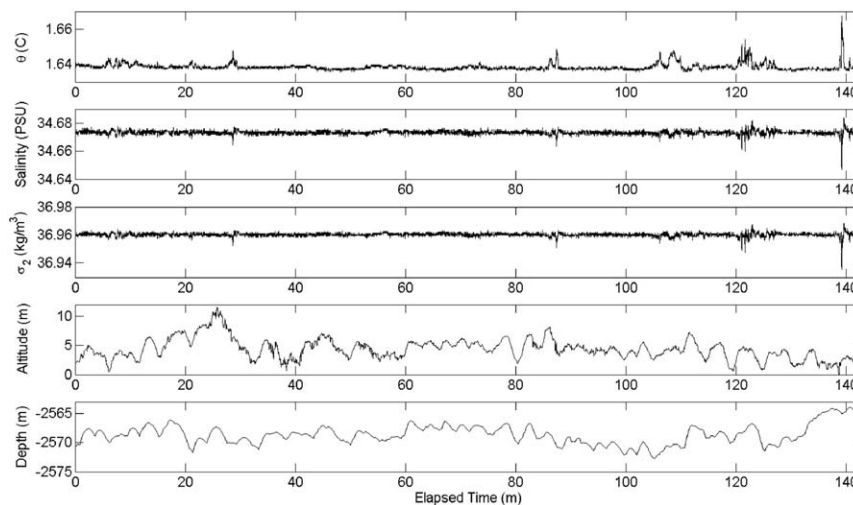


**Fig. 3.** Time series of potential temperature ( $\theta$ ), salinity, potential density anomaly ( $\sigma_2$ ), altitude, and depth during the injection. The data are from a SeaBird SBE 19 CTD and a Benthos PSA-900D altimeter mounted on *Alvin*. Table 1 gives the mean and standard deviation for these records.

**Table 1.** Statistics of the hydrography, altitude and depth during the tracer injection.

Variable	Mean	Std. deviation
$P$ (dbar)	2599	2.2
$T_{90}$ ( $^{\circ}\text{C}$ )	1.8243	0.0020
$\theta$ ( $^{\circ}\text{C}$ )	1.6366	0.0020
$C$ (mS/cm)	–	0.0018
$S$ (PSU)	34.6720	0.0015
$\sigma_2$ ( $\text{kg}/\text{m}^3$ )	36.9592	0.0013
Altitude (m)	4.3	1.8
Depth (m)	2564	1.6

temperature fluctuations along the injection reach, noted above as  $3 \times 10^{-4} \text{ kg}/\text{m}^3$ . Hence, this last number remains the lower limit to the initial density spread. We present evidence later that in fact some of the tracer was mixed into considerably lighter water early in its history by entrainment into the plume of K-vent, a high-temperature vent located along the injection reach.

The estimate of the mean density of the initial tracer plume is affected by uncertainty in the salinity calibration of the SeaBird 19 CTD on *Alvin*. This CTD was intercalibrated with the SeaBird SBE 9plus used for the CTD casts during both the deployment cruise and the sampling cruise (LADDER 2; 11 December 2006 to 5 January 2007), and the SBE 9plus was calibrated with a Guildline Portasal salinometer on *Atlantis* on both cruises, using samples taken from Niskin bottles. Uncertainty in the salinity calibration across cruises is approximately 0.001 and in potential density is therefore  $0.0008 \text{ kg}/\text{m}^3$ . We have set the inter-cruise calibration, within this uncertainty, such that the mean density of the injection matches the peak of the tracer distribution found during the survey cruise.

### 2.5. Velocity measurements at the injection site

An array of current meters was deployed during LADDER, both along the ridge crest and on the flanks of the ridge. The record of most interest for the early stages of the tracer experiment was from a Teledyne RDI Workhorse 300 kHz Bottom-Mounted Acoustic Doppler Current Profiler (BMADCP) deployed from DSV

*Alvin* in the axial summit trough. It was positioned near  $9^{\circ}30'\text{N}$ , approximately at the center of the tracer injection streak, on 31 October 2006, and recovered on 15 December 2006. The range of good observations is from 8.5 meters above bottom (mab) to nearly 100 mab (4 m bins, 20 min ensembles).

The first valid bin of the BMADCP is near the top of the AST where cross-axis flows are likely to be stronger than within the AST (Fig. 4). During the injection and the 12 h following it, the zonal component of the current in this bin was to the west from 5 to 10 cm/s. The meridional component was weaker with a predominately southward flow during the first 18 h and predominately northward flow for the second 18 h period.

The progressive vector diagram (PVD) for the full 33-day deployment shows a northwestward flow at the time and site of the injection, continuing for approximately 25 days, at which time the flow gradually reversed, turning back to the southeast (Fig. 5). The southeastward subinertial flow continued for approximately 9 days before the BMADCP was recovered. Current meters deployed near the BMADCP during LADDER 1 and recovered a year later during LADDER 3, in October 2007 are consistent with the BMADCP data. However, current meters deployed during the same time period on the western flank of the ridge, show much weaker flows, though in the same sense, i.e., northwestward followed by southeastward. These current meter data will be reported elsewhere.

### 3. Tracer survey

The tracer survey began on 14 December 2006 and ended on 3 January 2007, and thus occupied the period between 32 and 52 days after release. The survey was performed with both a conventional CTD/Rosette with 10 L Niskin bottles, and with a set of five 1.2 L Niskin bottles mounted on *Alvin* and tripped within a few meters of the bottom. In both cases water was transferred to 500 ml glass bottles with ground glass stoppers and these bottles were stored under cold water prior to analysis. In all, 100 CTD casts were performed (including 2 shallow casts for testing) and 37 samples from *Alvin* were collected in three stages of the survey (Table 2).

SF<sub>6</sub> concentrations were measured for each bottle sample using a gas chromatograph with an electron capture detector

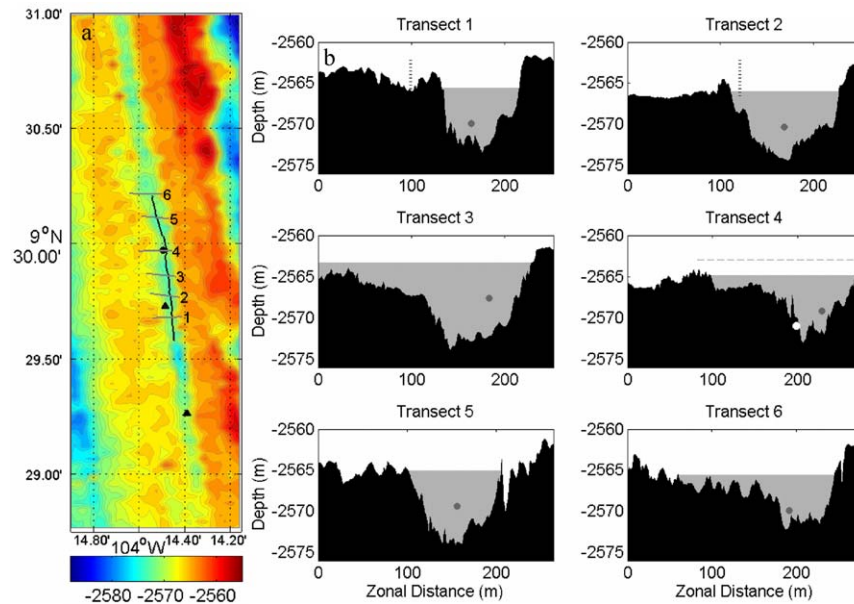


**Fig. 4.** Injection site and initial plume at 9°30'N on the EPR. (a) Dive Track for dive 4271 (black line). The tracer was injected with the submersible moving from north to south in the AST. Bathymetric survey transects from dive 4259 are shown as grey lines across the AST. A bottom-mounted ADCP (black circle) and the locations of known vents (triangles; north, K-vent; south, PBR-600, discovered during LADDER 1) are also shown. The bathymetric contour interval is 1 m. (b) Cross sections of the AST from the numbered transects in (a). The shaded region shows the estimated extent of the initial tracer plume in each section. The stacked lines in transects 1 and 2 show K-vent, which is 4–5 m tall and lies between these two transects. The dark grey spot marks the location of the injection orifice, mounted on *Alvin*, as it passed through each cross section. Transect 4 shows the location of the BMADCP (white circle) and the depth of the midpoint of the first valid velocity bin (grey dashed line).

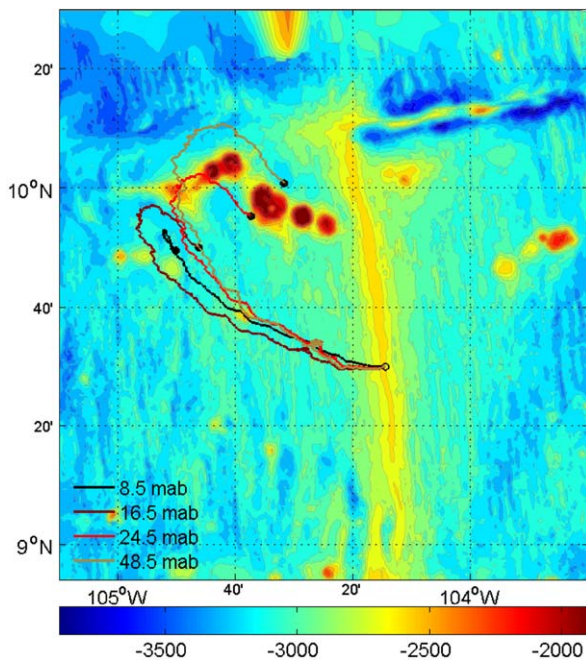


**Fig. 5.** Progressive vector diagram for selected bins (8.5–48.5 m above bottom) from the BMADCP record starting at the time of the injection (17:07 GMT 12 November 2006) through the end of the record (17:00 GMT 15 December 2006).

following the methods of Law et al. (1994) within hours of sampling. There was an analysis system blank during this cruise of 0.15 fM, symptomatic of a small leak of laboratory air into the evacuated part of the system used to sparge the sample. Concerted efforts failed to find and fix this leak, however. Variations in the sample blank during the cruise are estimated

**Table 2.**

Tracer survey schedule.

Stage	Days	Casts	Methods
1	14 December–18 December 2006	2–12	<i>Alvin</i> , CTD/LADCP
2	18 December–28 December 2006	13–82	CTD/LADCP
3	28 December 2006–3 January 2007	83–100	<i>Alvin</i> , CTD/LADCP

at less than 0.04 fM, based on samples taken outside the tracer patch. The uncertainty in concentrations from the CTD/Rosette is therefore the larger of 0.04 fM or 2% of the concentration, the latter number arising from volumetric and chromatographic sources of error.

Uncertainty in the concentrations from *Alvin* samples is much larger because of the small size of the 1.2 L Niskin bottles. Bubbles can form more easily than in the 10L bottles during ascent through warm upper waters, due to the smaller ratio of surface to volume. More seriously, the 500 ml glass sample bottles, which are usually flushed with 1000 ml of water before closing with their glass stoppers, could not be flushed properly due to the paucity of water, and so the *Alvin* samples suffered air contamination during transfer. Water at equilibrium with the air at 17 °C, the approximate temperature of the 1.2 L Niskin water on deck, would have been 1.2 fM. The minimum concentrations measured in these samples were around 0.1 fM, and this level could be due entirely to contamination. Therefore, an uncertainty of 0.1 fM has been assigned to these samples, and concentrations between 0.1 and 0.3 fM have been interpreted cautiously.

### 3.1. Horizontal tracer distribution

Due to the large scale flow reversal during the tracer survey, which brought tracer back toward the ridge (Fig. 5), it was

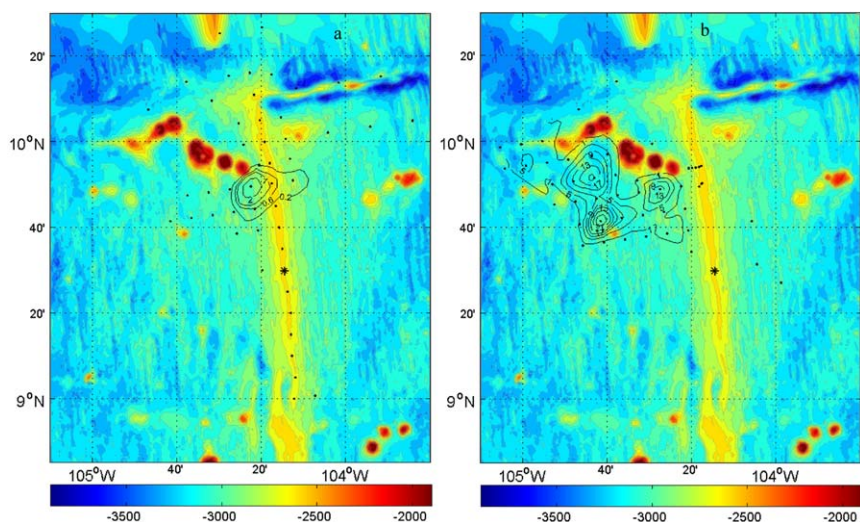


**Fig. 6.** Column integrals of tracer concentration ( $\text{nmol}/\text{m}^2$ ) 32–52 days after the release at  $9^\circ30'\text{N}$  on the EPR. The tracer contours overlay the SeaBeam bathymetry of Macdonald et al. (1992). (a) Tracer distribution for CTD stations 1–53 of the LADDER 2 cruise (14–24 December 2006, 32–42 days after injection). (b) Tracer distribution for CTD stations 54–100 (24 December 2006 to 03 January 2007, 42–52 days after injection). Note the difference in contour intervals between the two plots (a: irregular contour interval,  $2 \text{ nmol}/\text{m}^2$  maximum; b: contour interval =  $4 \text{ nmol}/\text{m}^2$ ,  $25 \text{ nmol}/\text{m}^2$  maximum). Column integrals less than  $0.2 \text{ nmol}/\text{m}^2$  are not shown. The CTD stations are shown as black dots and the injection site is marked with a star.

necessary to break the survey into two periods for analysis. The first period spans casts 1–53 and includes days 32–42 after the injection. The second period spans casts 54–100 and includes days 42–52 after injection. This division was made at cast 54 to separate casts made at repeated stations south of the Lamont seamounts at which tracer was found on the second occupation but not on the first. Tracer inventories were estimated by multiplying the column integral at each station by the square of the distance between stations (typically 9 km) and summing.

During the first survey period approximately 3% of the tracer was located, mostly in a patch on the flank of the ridge west of the  $9^\circ50'\text{N}$  vent site, i.e. nearly 40 km north of the injection site (Fig. 6a). This patch extended east across the ridge crest at  $9^\circ50'\text{N}$ . Tracer concentrations rapidly dropped to background values within 20 km to the west of the ridge. Small concentrations of tracer were also detected along and near the ridge axis north  $9^\circ50'\text{N}$ ; the total mass of tracer found north of the Lamont Seamounts was about 10 g, or 0.3% of the tracer injected, and not visible in the contours of Fig. 6a. Moderate concentrations of tracer were detected near the injection site at  $9^\circ30'\text{N}$  in too small an area to appear in Fig. 6a. The total mass in the original injection reach, estimated from one cast there, was on the order of  $10^{-3}$  g, and confined primarily to the AST, suggesting that small amounts of tracer trapped in collapse pits or in the sediment at the time of injection were still bleeding out (see Section 3.3).

A second patch of tracer, accounting for approximately 57% of the tracer, was detected south of the Lamont Seamounts during the second period of the survey (Fig. 6b). This patch extended 30 km south of the seamounts and more than 80 km west from the EPR ridge axis. Large amounts of tracer were found at stations where no tracer had been detected during the first survey period, i.e., the westernmost stations in Fig. 6a. The tracer patch appeared to be moving back toward the ridge, perhaps from the western end of the seamounts, over the course of the overall survey. The southeastward advection of the tracer patch is consistent with the subinertial currents measured at the injection site during the same period (Fig. 5), though, as mentioned earlier, currents measured off-axis by the mooring array were much weaker than those at the ridge crest. Finally, no tracer was found either at the stations south of the injection site or to the east along the Clipperton Fracture Zone (CFZ) at  $10^\circ10'\text{N}$ .

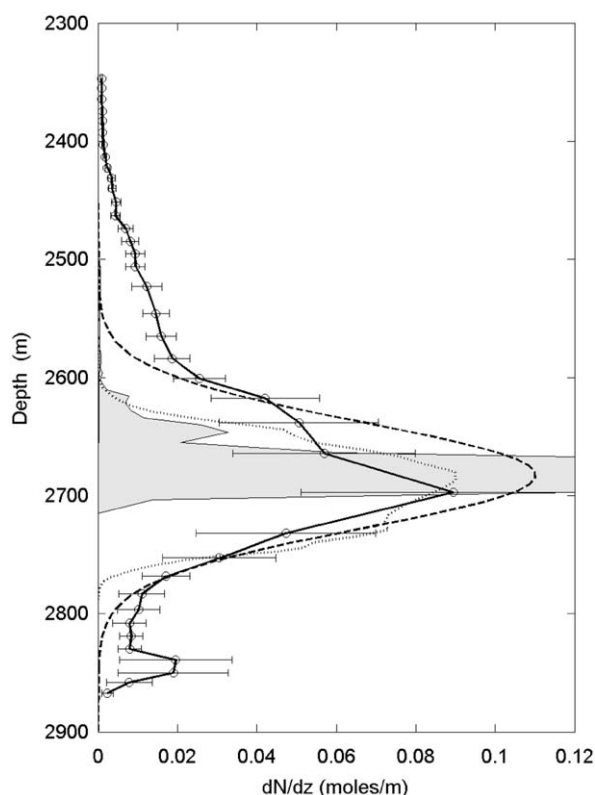


**Fig. 7.** Vertical tracer distribution constructed from 98 tracer profiles (solid line with error bars). The tracer has been summed in density bins and then plotted versus depth using the mean density profiles for the 10 LADDER 2 stations that reach the greatest density. The grey filled profile shows the initial distribution of tracer based on the temperature measured during injection. Its peak is off the graph at  $0.34 \text{ moles}/\text{m}$ . The dashed line is a Gaussian curve corresponding to a vertical diffusivity of  $2 \times 10^{-4} \text{ m}^2/\text{s}$  in the absence of boundaries and plumes (see text). The dotted curve shows distribution 1 from Fig. 13, transformed into depth coordinates.

The northwest boundary of the tracer patch was not delimited due to time constraints. We hypothesize that much of the tracer not accounted for was to the north and west of the seamounts. The incompleteness of the inventory does not seriously affect our

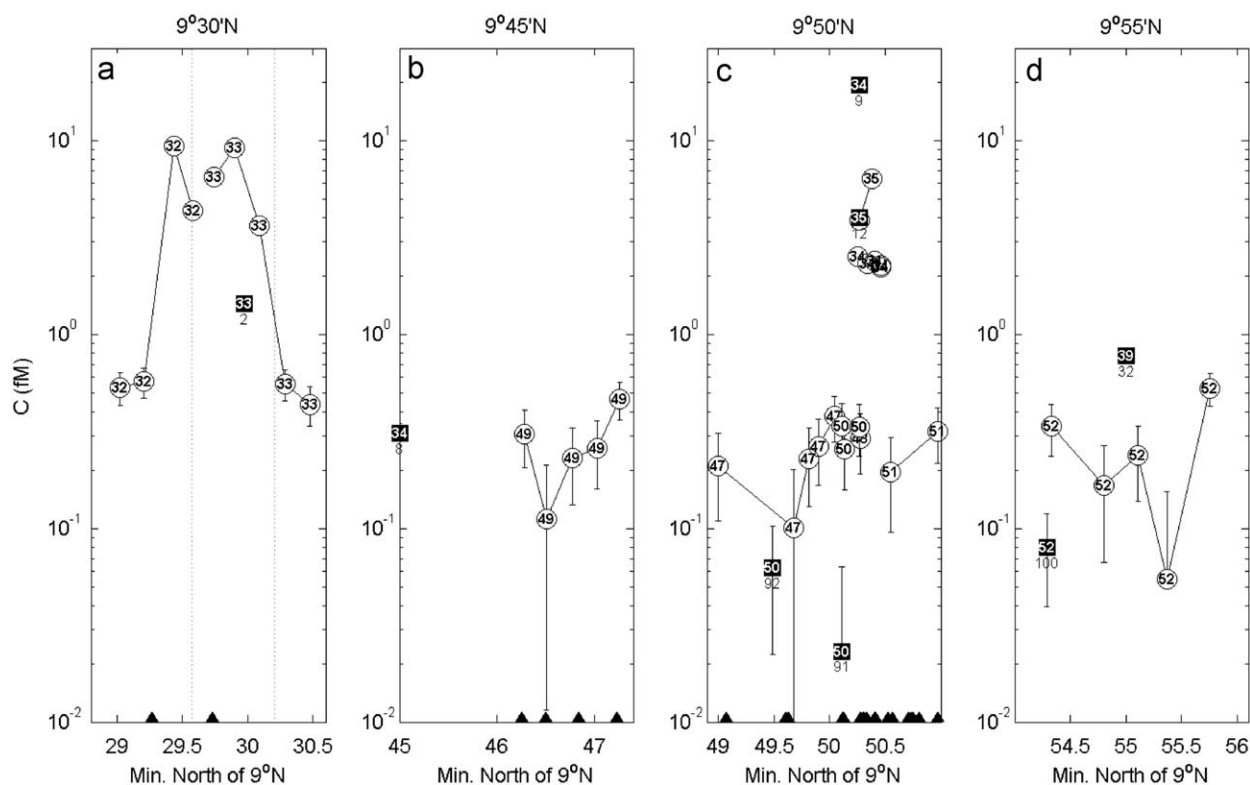


**Fig. 8.**  $\text{SF}_6$  concentrations in four regions along the ridge crest. Circles indicate *Alvin* samples in the AST\*, while squares show the concentration of  $\text{SF}_6$  in the deepest CTD samples in the same regions (5–15 mab). Numbers within the symbols give the time since injection, in days. LADDER 2 cast numbers are indicated below the squares. *Alvin* samples are contaminated by air invasion during sampling, such that concentrations on the order of 0.1 fM are suspect. Black triangles along the abscissa show the locations of known vents and the grey lines in the leftmost panel show the boundaries of the tracer injection. \**Alvin* samples in panel d, near 9°55'N, were taken east of the ridge axis in an adjacent trough formed by the fissure ridge and the first fault scarp (see Fig. 9).

goal of studying mechanisms of larval dispersion along the ridge, although it does introduce uncertainties in the distribution of tracer as a function of density and, in particular, estimates of the diapycnal diffusivity and of the amount of tracer entrained into buoyant vent plumes.

### 3.2. Vertical tracer distribution

A tracer inventory in density space was constructed from individual tracer profiles at all stations by breaking the profiles into density layers, and summing the product of the mean tracer concentrations, layer thicknesses, and representative area for each station. The resulting tracer inventory in density space was then mapped to depth space (Fig. 7) by using a mean density profile derived from 10 off-axis casts spanning the broadest range of densities. This density profile is representative of the far field, but not of the region within 10 km or so of the ridge crest. In particular, in this far-field profile the depth of the isopycnal surface of the tracer injection is approximately 120 m greater than the actual depth of the injection.

The filled grey curve in Fig. 7 represents the distribution of tracer based on the CTD temperature during injection. Its peak is off scale, at 0.34 moles/m. The dashed curve in Fig. 7 is a Gaussian curve centered at the peak of the injection distribution and normalized to the same total mass as the other curves. This is approximately the distribution the tracer would have in LADDER 2 if it had diffused from the LADDER 1 profile in the absence of boundaries with a depth-independent diffusivity of  $2.0 \times 10^{-4} \text{ m}^2/\text{s}$ . Below about 2700 m the Gaussian curve fits the observations fairly well, except at the very bottom where the presence of the bottom boundary makes itself felt in raising the tail of the observed

distribution by shutting off downward diffusion. The secondary peak near 2850 m can only be explained with a complex lateral distribution of the tracer, coupled with incompleteness of the tracer survey. We consider  $2 \times 10^{-4} \text{ m}^2/\text{s}$  to be a reasonable estimate for the diffusivity affecting the lower half of the tracer patch, since the wake of *Alvin* and vent plumes will only carry tracer to lighter, shallower levels in this plot, rather than denser levels.

The situation above 2700 m is quite different. It appears that a sizeable fraction of the tracer has been transferred from near the center of the distribution to the upper shoulder near 2630 m and upper tail above 2600 m depth. This transfer is unlikely to be due to diapycnal mixing, which one would expect to decrease with height above the bottom. Rather, we conclude that tracer has been transported upward by entrainment into hydrothermal plumes of the diffuse sources and of K-vent in the vicinity of the injection streak. This entrainment is explored in detail in Section 5.

Spatial patterns in the vertical distribution of the tracer suggest vertical variations in the strength of the circulation outlined earlier. Most notably, a deep layer of tracer, contributing to the deep secondary peak in Fig. 7, appeared to lag behind to the west as the main body of the tracer moved back to the east, and a shallow layer of tracer, contributing to the upper shoulder and tail mentioned above, was concentrated in stations toward the northern part of the patch within 20 km of the seamounts. Tracer that had made the most progress back toward the ridge by the end of sampling was concentrated near the center of the distribution.

### 3.3. Tracer concentrations in the axial summit trough

Tracer concentrations measured within the AST were highest near the 9°30'N injection site and the 9°50'N vent sites early in

the tracer survey (Fig. 8). As mentioned earlier, elevated tracer concentrations at the injection site 32 to 33 days after the injection were most likely due to a slow release of tracer trapped in collapse pits and fissures during the injection, or tracer bleeding from the sediments, since the concentration was undetectable more than 20 m above the bottom of the AST and in surrounding stations. Of much greater interest for the question of larval dispersal are concentrations of 2–7 fM found in samples taken by DSV *Alvin* in the AST at 9°50'N, 34 to 35 days after the release (Fig. 8c). These samples demonstrate that tracer originating in the AST at 9°30'N can indeed be found in the AST 20 nautical miles north at 9°50'N within the life span of vent larvae such *Riftia pachyptila*.

High tracer concentrations were also found just above the AST at 9°50'N in CTD/Rosette samples. Samples from casts 9 and 12, taken on days 34 and 35, i.e., the same days as the *Alvin* samples just discussed, reveal fairly homogeneous layers of tracer with concentrations of 19 and 4 fM, respectively, between 5 and 50 mab (Fig. 8c). Temperature and turbidity data from these casts clearly showed the presence of vent plumes in this same 50 m layer (see Fig. 13b).

Tracer concentrations in the AST near 9°50'N in the second period of the survey, 42–53 days after injection, were an order of magnitude lower than during the earlier period (Fig. 8). During both periods, though, tracer concentrations in the axial trough often exceeded those just above the trough, supporting the idea that the AST can retain tracer passing across it, at least for short periods of time. This idea is furthermore supported by temporal changes in the tracer pattern. In-trough concentrations at 9°50'N increased from 2 to 5 fM between days 34 and 35, while concentrations just above the trough decreased from 20 to 4 fM during the same period. Evidence for retention in steeply bounded

depressions was also found from *Alvin* samples in a trough running parallel to, and just to the east of, the AST near 9°55'N (Fig. 9). Concentrations in this trough (at 9°54.31'N and 9°55.75'N in Figs. 8d and 9) were greater than those near the top of the ridge just to the west (between these two latitudes in the figures).

#### 4. Vent plume observations

Hydrothermal fluids enter the deep ocean in focused, high-temperature jets issuing from small sulfide orifices, and in distributed, low-temperature plumes from diffuse sources (Baker et al., 1993). These low-density fluids form buoyant plumes that rise through and entrain the ambient water until the plume density equals that of the background and the plumes spread laterally at their level of neutral buoyancy, which is typically between 100 and 300 meters above bottom (mab) for high-temperature discrete vents (e.g. Baker et al., 1994) and less than 50 mab for low-temperature diffuse sources (Rona and Trivett, 1992). The rise height of vent plumes depends on the buoyancy flux at the source, the background density stratification, and the magnitude of cross-flows (Morton et al., 1956; Lavelle, 1997). Neutrally buoyant plumes are often mixtures of fluids from discrete and diffuse sources and ambient water (Lavelle and Wetzler, 1999).

##### 4.1. Overview of neutrally buoyant plumes

Of the 136 CTD profiles completed during the two cruises, 29 revealed pronounced peaks in turbidity which we identify with hydrothermal vent plumes (locations are shown in Fig. 1 and listed in Table 3). Some casts had multiple turbidity peaks, which

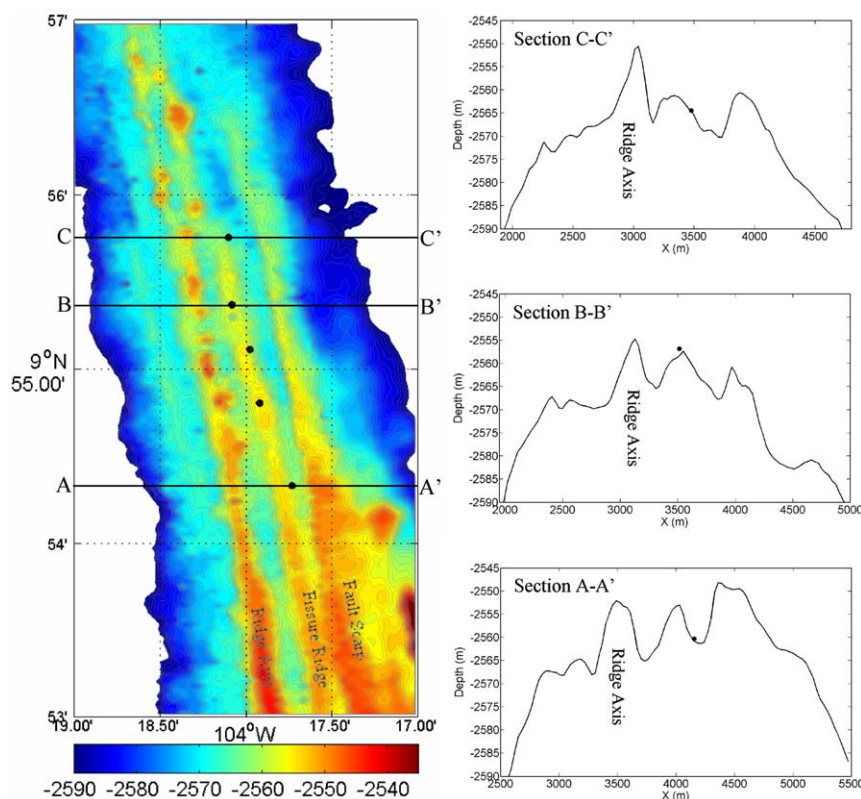


**Fig. 9.** Bathymetry of the summit of the East Pacific Rise at 9°55'N. Tracer samples collected with *Alvin* on dive 4296 (3 January 2007) are shown as black dots. Concentrations are shown in Fig. 8d. The depth contour interval is 1 m. Cross-sections are shown on the right for three of the samples (black dots). Multibeam bathymetry (EM300) is from White et al. (2006).

**Table 3.**

CTD casts in which hydrothermal plumes were detected. The rightmost column gives the height above bottom (HAB) of the deepest sample in the cast.

LADDER cruise	Cast	Date (GMT)	Time (GMT)	Days after injection	Lat	Lon	Bottom depth (m)	HAB of deepest sample (m)
1	4	1-November-06	10:08	–	9.83346	–104.29219	2503	1
1	10	4-November-06	7:40	–	9.88358	–104.34150	2838	6
1	12	5-November-06	7:49	–	9.49980	–104.24141	2562	27
1	13	6-November-06	1:28	–	9.49669	–104.33061	2782	25
1	14	6-November-06	4:40	–	9.50001	–104.24171	2561	22
1	16	7-November-06	0:52	–	9.49667	–104.32933	2784	18
1	19	8-November-06	9:44	–	9.66733	–104.26100	2536	25
1	23	10-November-06	8:10	–	9.58335	–104.25167	2536	22
1	26	12-November-06	6:08	–	9.58283	–104.25167	2543	28
1	28	13-November-06	7:59	1	9.50000	–104.32999	2790	43
1	30	14-November-06	4:19	2	9.15008	–104.21116	2596	29
1	31	14-November-06	9:50	2	9.66681	–104.26471	2535	35
1	33	15-November-06	7:25	3	9.74937	–104.27513	2527	28
1	34	15-November-06	10:12	3	9.66676	–104.26112	2536	37
2	2	15-December-06	0:28	33	9.49963	–104.24177	2566	2
2	3	15-December-06	3:48	33	9.41667	–104.23000	2571	1
2	6	16-December-06	1:05	34	9.58333	–104.25070	2547	4
2	8	16-December-06	7:00	34	9.75000	–104.27547	2528	8
2	9	16-December-06	9:58	34	9.83783	–104.29133	2500	6
2	12	17-December-06	10:06	35	9.83788	–104.29135	2501	7
2	26	19-December-06	14:08	37	9.16667	–104.21195	2577	6
2	27	20-December-06	3:38	38	9.08333	–104.19807	2608	7
2	28	20-December-06	6:36	38	9.00000	–104.20338	2649	15
2	32	20-December-06	9:37	38	9.64322	–104.42962	2547	6
2	33	21-December-06	5:51	39	10.00000	–104.32019	2551	7
2	83	29-December-06	9:07	47	9.83788	–104.29135	2500	11
2	88	31-December-06	2:41	49	9.57162	–104.33410	2819	16
2	91	1-January-07	7:07	50	9.83517	–104.29433	2512	15
2	100	3-January-07	10:31	52	9.90483	–104.29550	2551	1

for simplicity we count as separate plumes, though we recognize that spatial variability in a single plume can lead to multiple turbidity peaks (e.g. Thurnherr and Richards, 2001). Of the 65 observed hydrothermal plumes so counted, 40 were stable, i.e., the potential density decreased with height throughout, and thus had reached their level of neutral buoyancy. While a majority of the plumes were detected over the ridge axis, neutrally buoyant plumes were detected up to 9 km off-axis on the western flank, and several plumes were detected near the overlapping spreading center near 9°00'N (see Fig. 1).

Fig. 10 shows the turbidity-weighted mean depth and the range of depths occupied by the neutrally buoyant plumes, and Fig. 11 shows the same in density space. Plume numbers are assigned along the abscissa of these graphs in a manner that groups the plumes by region, while each plume is also marked with the cast number for reference to Fig. 1. Plume depths and thicknesses match those recorded by Baker et al. (1994) in spite of changes to the vent fields due to the 2006 eruption (Tolstoy et al., 2006) and the transient nature of vents (Fig. 10).

#### 4.2. Plumes near 9°30'N

The range of depths and densities for the neutrally buoyant plumes show only small variability with position along the ridge or between cruises. Plumes observed near 9°30'N during LADDER 1 were at greater densities, but not much greater depths, than those observed farther north along the ridge segment. The spatial variability in plume characteristics seen during LADDER 1 was mainly due to the observation of several deeper plumes 9 km off-axis on the western flank at 9°30'N (Fig. 10, plume numbers 3, 7, and 13; casts 13, 16, and 28). Baker et al. (1994) also found plumes on the western flank near 9°30'N to be relatively deep. The off-axis plumes observed during LADDER 1 reside, however, on the same density surfaces as the on-axis

plumes near 9°30'N (Fig. 11, plume numbers 2, 5, 9, and 11; LADDER 1 casts 12, 14, 23, and 26). Plumes near 9°30'N are relevant to the discussion of tracer entrainment in Section 5, since one likely source of these vents is K-vent, which was along the injection reach.

#### 4.3. Plumes near 9°N

While of no concern for the tracer study, it should be noted that LADDER 2 casts 26, 27 and 28 from 9°00'N to 9°10'N along the eastern limb of the 9°N overlapping spreading center (OSC) revealed thick plumes with turbidity signals comparable to plumes detected in off-axis casts near 9°30'N. The plumes were over 200 m thick, spanned a large range of densities, and were located 150–250 mab, suggesting a high temperature source (Figs. 10 and 11, plume numbers 23, 24, and 25). Baker et al. (1994) found only a very weak plume signal on the eastern limb and a slightly stronger signal on the western limb of the OSC, yet camera tows revealed no evidence of active venting. Likewise, camera tows in 1986 over the 9°N OSC revealed no vent activity (Sempere and Macdonald, 1986). The present observation of plume signals on the eastern limb of the 9°N OSC suggests that active vents may have developed in recent years.

### 5. Tracer entrainment into buoyant plumes

#### 5.1. K-vent

The only known vent along the injection reach of the AST is “K-vent”, though temperature anomalies along the injection track indicate the presence of diffuse flows of warm water all along the injection track (Fig. 3). K-vent, a 5 m tall mushroom-shaped sulfide structure, is located at 9°29.73'N, 104°14.484'W, along the

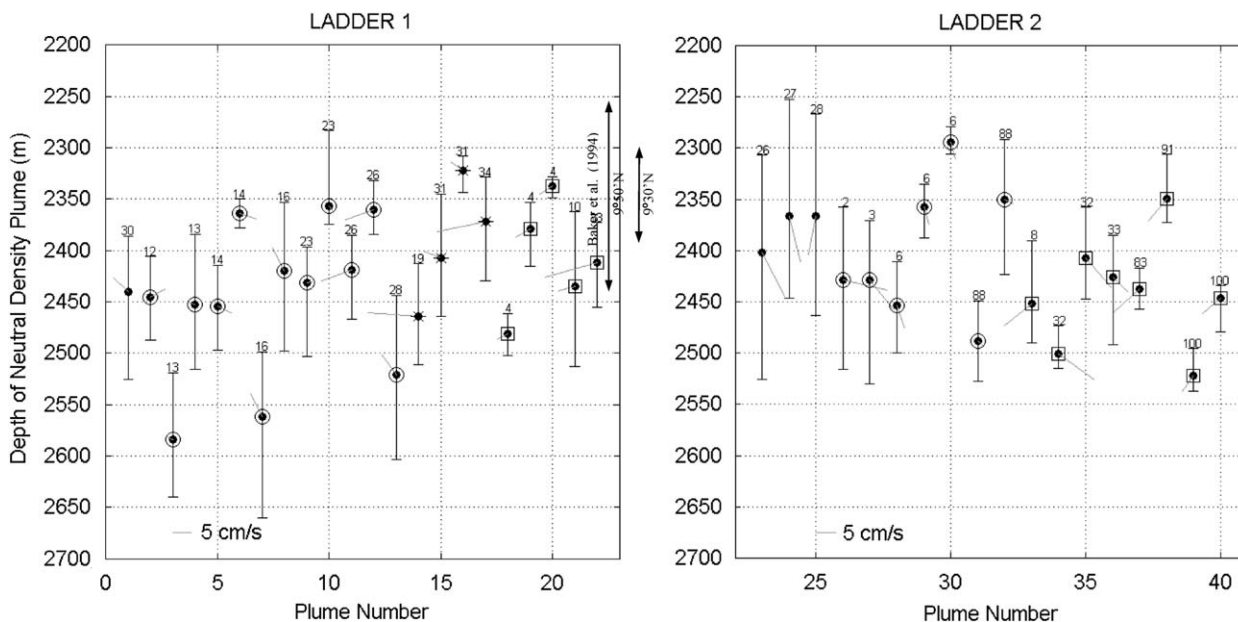


**Fig. 10.** Distribution of depths of neutrally buoyant hydrothermal plumes detected in CTD casts on LADDER 1 and LADDER 2 along the East Pacific Rise. Dots show the turbidity-weighted mean depth of the neutral buoyancy layer for each plume and bars indicate the upper and lower limits of the plume. Geographical locations (within a 12 km radius) are designated by open symbols around closed dots (circles, 9°30'N; stars, 9°40'N; squares, 9°50'N; none, 9°05'N). The plume number is shown along the abscissa. The CTD cast number is shown above each point; there is more than one plume shown for some casts. Grey lines originating from each point show the mean current speed and direction below the neutral density depth from a Lowered ADCP deployed with the CTD (North is to the top). Plume observations of Baker et al. (1994) for the EPR are shown for reference between the panels.

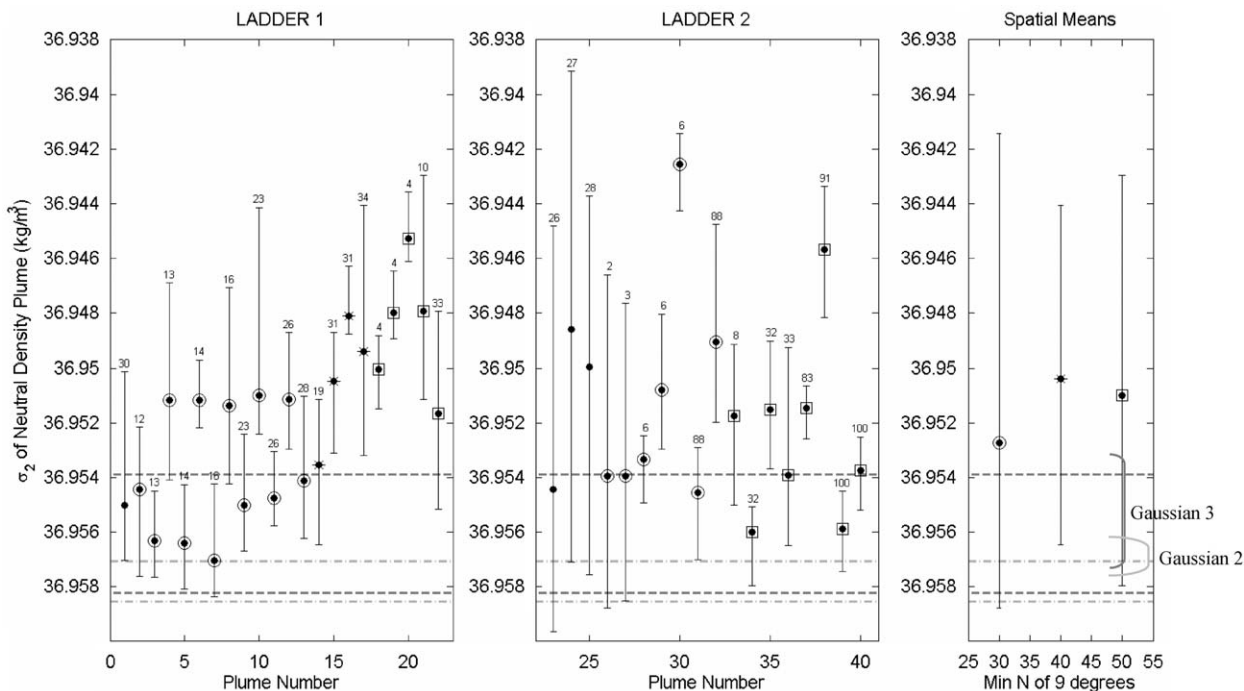


**Fig. 11.** Potential density distribution of neutrally buoyant hydrothermal plumes detected in CTD casts on LADDER 1 and LADDER 2 along the East Pacific Rise. The turbidity-weighted mean and range of potential densities (referenced to 2000 m) observed in each plume (detected from turbidity) are shown. Symbols and annotations are the same as in Fig. 10. The right panel shows the geographic mean of the neutral density plumes detected near 9°30'N, 9°40'N and 9°50'N with bars showing the maximum extent of plume observations. Limits of Gaussian distributions 2 and 3, described in Section 5.2, are shown for reference ( $\pm 2$  standard deviations).

western wall of the AST (Figs. 4 and 12). Surrounding the base of the vent at a depth of about 2567 m were extinct chimney structures and patches of warm plumes from 30 cm to 1 m in diameter. Effluent temperatures in these patches ranged from 10 to 30°C and the effluent velocity, estimated from video images,

was 1–3 cm/s. The top of the main structure spanned depths from 2562 to 2564 m and was characterized by more vigorous hydrothermal venting of clear and grey smoky water at temperatures between 10 and 150°C. Six dives covering the entire length of the injection region failed to find any other significant sites of

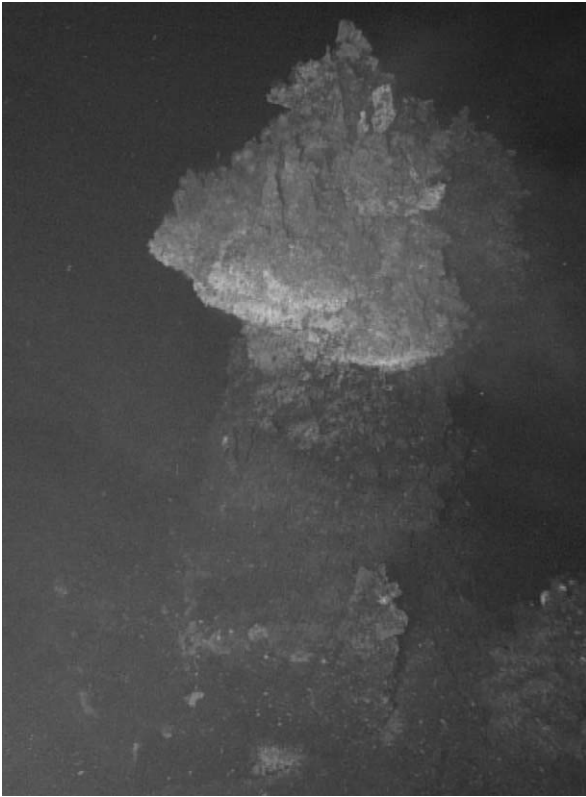


**Fig. 12.** Photo mosaic of K-vent from video obtained on *Alvin* dive 4272, provided by S. Beaulieu. Some of the cloudiness of the water was created by the submersible. The structure is 4–5 m tall.

high-temperature hydrothermal venting, although smoky water observed just south of K-vent suggested the possible existence of another vent nearby.

Estimates of the initial tracer plume suggest that the bottom half of K-vent was immersed in tracer-rich water (Section 2.4). Based on video evidence, the diffuse flows around the base of K-vent could have entrained tracer and provided it with sufficient vertical momentum to be entrained into the main plume from K-vent. The westward cross-axis flow observed during and immediately after the tracer injection (Section 2.5) may have swept tracer up the west wall of the AST and across K-vent, adding to the entrainment.

### 5.2. An estimate of the tracer entrained into plumes

In Section 3.2 we suggested that entrainment into hydrothermal plumes was responsible for moving tracer into the upper shoulder and tail of the vertical tracer distribution (Fig. 7). As noted above, K-vent probably played a major role in this entrainment. In an attempt to quantify the entrainment, we have fit the tracer inventory in density space with a superposition of 3 Gaussian distributions using a nonlinear least squares fitting routine (Fig. 13 and Table 4). Distribution 1 in Fig. 13, representing about 38% of the tracer injected and an estimated 64% of the tracer found, captures the center of the observed tracer distribution, but not the upper and lower tails. Distribution 1, transformed into depth coordinates, is also shown as the dotted curve in Fig. 7. This curve is narrower than the dashed curve in Fig. 7, and corresponds to a value of  $0.4 \times 10^{-4} \text{ m}^2/\text{s}$  for diapycnal diffusivity. However, distribution 1 does less well than the dashed curve in Fig. 7 at fitting the deep tail of the overall tracer distribution, even though the center of distribution 1 lies below

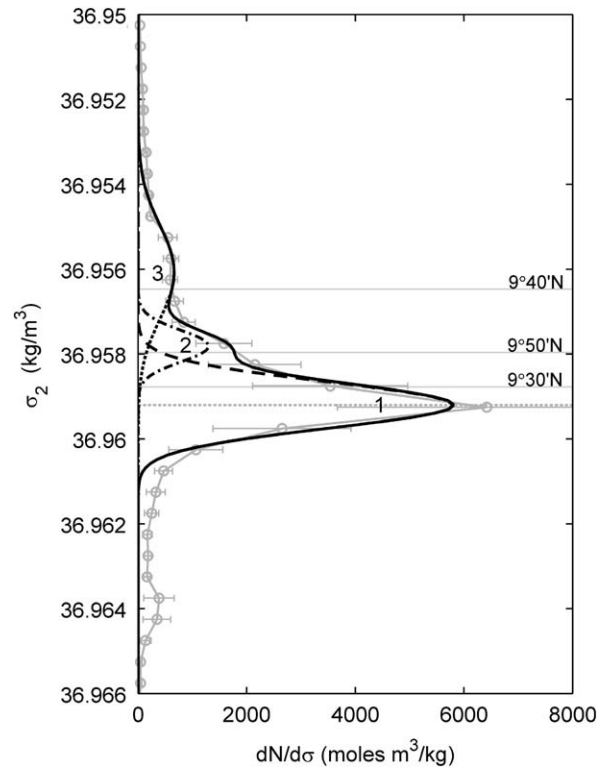


**Fig. 13.** Tracer distribution in density space (grey curve with error bars) with a nonlinear least squares fit to the main peak and the upper tail. The fit comprises the superposition of three Gaussian distributions. Distributions 1 (dashed line), 2 (dash-dot) and 3 (dotted) are found to give the best fit (solid black line) to the upper half of the tracer distribution (grey circles). The grey dotted line is drawn through the peak of the distribution. The solid grey horizontal lines show the highest potential density observed in the vent plumes located near 9°30'N, 9°40'N and 9°50'N.

**Table 4**

Characteristics of the Gaussian distributions in Fig. 13. The molar mass of  $\text{SF}_6$  is 146.05 g/mol.

Model distribution	Mean	Variance	Total tracer (g)	% Tracer injected
1	36.9592	2.913E-07	1146	38.2
2	36.9578	1.353E-07	176	5.9
3	36.9561	1.237E-06	271	9.0

the center of the dashed curve. Hence, as discussed in Section 3.2, we associate the estimate of  $2 \times 10^{-4} \text{ m}^2/\text{s}$  to the region below the tracer peak, i.e., closer to the bottom, while the value of  $0.4 \times 10^{-4} \text{ m}^2/\text{s}$  may be more appropriate for the central part of the tracer distribution.

Distributions 2 and 3, accounting for 10% and 15% of the tracer found, respectively, are intended to represent the effect of entrainment into vent plumes. These distributions are consistent with the distribution of densities observed in neutrally buoyant hydrothermal plumes found within 10 km of the injection site, and within days of the injection (plume numbers 2, 3, 5, 7, 9, 11, and 13 in Fig. 11). The density range of plumes 3, 7, and 13, observed 9 km west of the injection site agree particularly well with distribution 3. Highlighting this agreement, Fig. 14 compares the turbidity profile from cast 3 of LADDER 1 with distribution 3.

While distribution 3 matches a number of observed plumes, distribution 2 lies along the upper bound of the density range of the observed vents and is at greater densities than the mean neutral density of all the plumes. It is possible that sampling

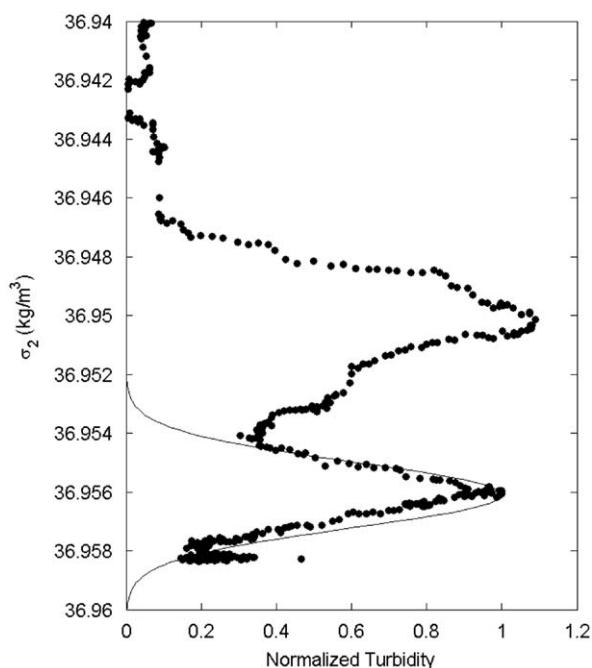


**Fig. 14.** Normalized turbidity profile in density space from off-axis cast 13 (LADDER 1) at 9°30'N. Turbidity (dots) was scaled by the local maximum in the deeper plume. The solid line is distribution 3 (see Fig. 13) scaled by its maximum value.

errors led to the shape of the upper shoulder of the tracer profile that necessitates the addition of distribution 2 to the 3-distribution fit. A more interesting, but also more speculative, possibility, however, is that the anomaly in the tracer profile associated with distribution 2 was due to plumes from diffuse sources that were not captured in the plume survey, due to their lack of turbidity. Our turbidity observations only account for the plumes of vents that produce particle-rich plumes by precipitating sulfides and metals upon cooling. Diffuse sources often produce little or no turbidity, either because mixing with ambient water causes sub-seabed precipitation or because diffuse effluent is simply heated seawater, with low-temperature vent fluid emitted as a clear, “shimmering” flow. As discussed in Section 2, the CTD on *Alvin* during the injection recorded numerous patches of water with temperature anomalies in the trough along the injection track (Fig. 3). Such temperature anomalies indicate the presence of diffuse flows in the area that would impart buoyancy to tracer. In addition, as discussed in Section 5.1, the area around K-vent had numerous patches of diffuse, shimmering flow capable of entraining tracer and contributing to distribution 2. Plume models (e.g., McDuff, 1995) indicate that the buoyancy flux in the AST required to produce a plume with density distribution 2 is on the order of  $10^{-4} \text{ m}^4/\text{s}^3$ , which is characteristic of low-temperature, diffuse sources.

In summary, we consider the part of the tracer profile represented by distribution 3 to be fairly clear evidence of entrainment of a substantial fraction of the tracer into hydrothermal vent plumes—probably from K-vent. Attribution of the part of the profile represented by distribution 2 is far less certain, but is suggestive of entrainment into diffuse source plumes in the segment of the AST in which the tracer was injected.

### 5.3. Observations of tracer in buoyant plumes

Entrainment of a significant fraction of the tracer into hydrothermal vent plumes was most likely to occur just after

the tracer injection, and the plumes involved would be from vents near the injection site, particularly the diffuse sources along the injection track and K-Vent, as described above. Later, the tracer was widely distributed, and encounters with vent plumes, though common, would involve only small fractions of the total amount of tracer and would have had little effect on the overall distribution of tracer with density. Nevertheless, observations of tracer in buoyant vent plumes all along the AST during LADDER 2 support the idea that tracer can be entrained from relatively dense water and lifted to lower densities by these plumes. Here we present the evidence for such entrainment, although we realize that our interpretation of the details are speculative in the face of unknown spatial and temporal variability in the tracer and turbidity fields.

Of the 16 CTD casts showing buoyant hydrothermal plumes along the ridge crest during LADDER 2, 8 showed correlations between turbidity and  $\text{SF}_6$  concentration. Fig. 15 shows four of these casts. At 9°35'N, 2.5 km north of the closest known vent (D-vent), cast 6 showed a broad turbidity plume with a tracer peak and a density inversion at its core (Fig. 15a). Cast 9 found a detached plume with a double peak in turbidity, but only a single tracer plume, which, however, extended to the seabed with approximately constant concentration (Fig. 15b). This profile, being at the center of the 9°50'N study site and very rich in tracer, was discussed in Section 3. The upper limit of the tracer patch was coincident with the upper limit of the deeper turbidity plume, suggesting that the thickness of the tracer patch was set by the rising hydrothermal plume. The concentration in an *Alvin* sample obtained only meters from the bottom CTD sample for this cast, and on the same day, was 8 times lower than in the CTD sample.

Cast 100, at 9°54'N, showed two distinct hydrothermal plumes that were well correlated with tracer plumes (Fig. 15c). While the turbidity signal dropped to background values near the bed, however, the tracer concentration was elevated in the bottom sample, taken at 5 mab. Nearby *Alvin* samples taken only hours after cast 100 revealed concentrations 4 times higher than in this bottom sample, suggesting a fairly concentrated, near-bottom patch of tracer feeding the vent plume (see Fig. 8d). Finally, at 10°N, cast 33 revealed a 50 m thick patch of tracer attached to the ridge crest and a second tracer maximum about 100 mab associated with the neutral density plume of an unknown vent (Fig. 15d).

## 6. Discussion

### 6.1. Flow scenario

The first phase of the tracer survey found a patch of tracer just west of the 9°50'N Integrated Study Site (Fig. 6a), and significant concentrations right on the ridge at this site as well. The concentration fell to zero as far as we looked to the west of this. Only 0.3% of the tracer was found north of the 9°50'N site, and the tracer concentration seemed to fall off rapidly to the east of the ridge. The second phase of sampling, however, found much of the tracer immediately south of the seamounts (Fig. 6b)—a large part of it where no tracer had been found during the first phase. Time did not allow us to find the western edge of the tracer patch. It seems likely that the main body of the tracer had traveled far to the west and then had come back towards the ridge due to the reversal of subinertial currents recorded by the BMADCP (Fig. 5).

One scenario for the path taken by the tracer is that, after being swept westward off the ridge axis shortly after injection, it moved northward along the western flank of the ridge until it turned west under the influence of the seamount chain. A northward flow on the order of 5 cm/s along the western ridge flank was

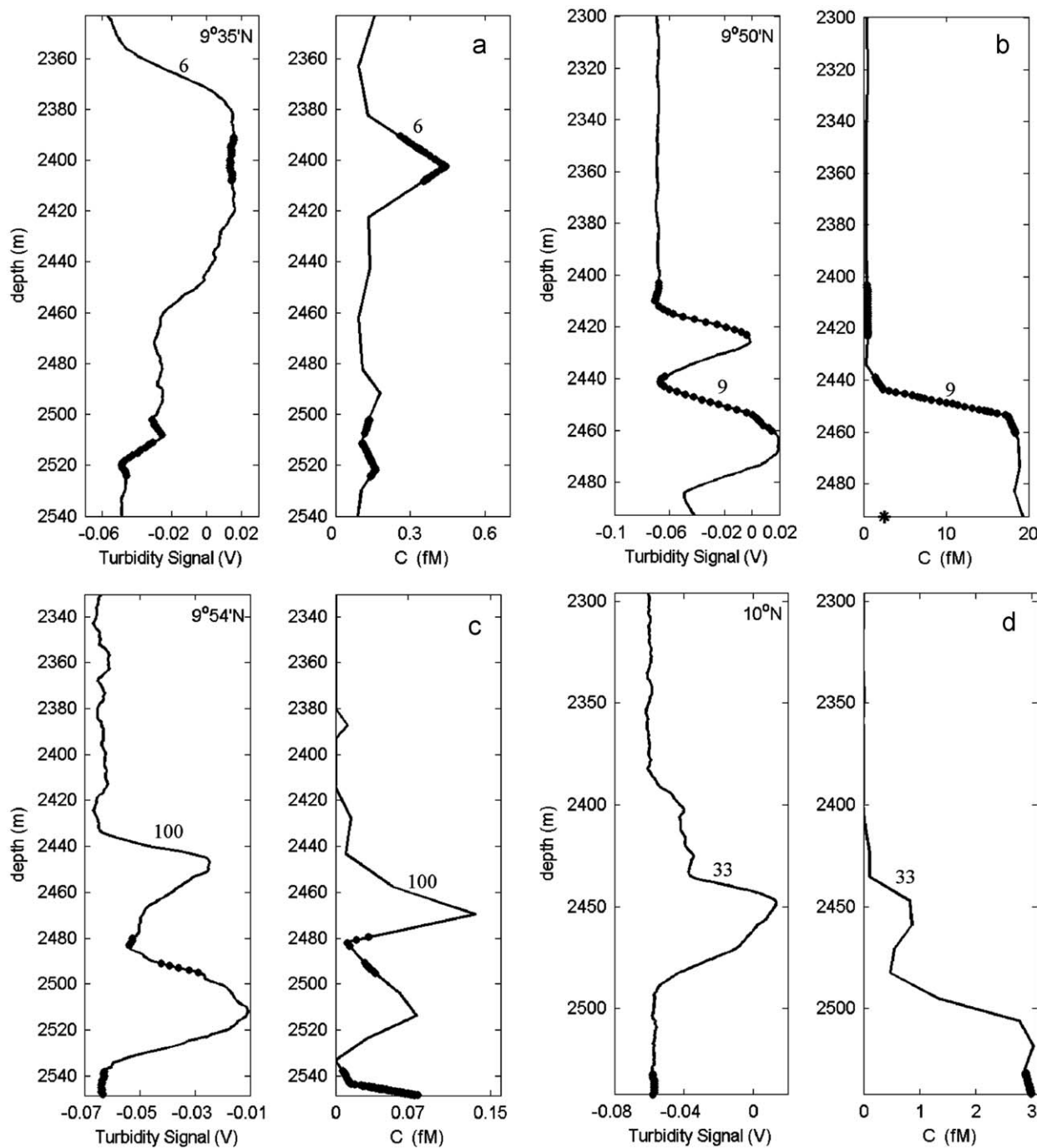


**Fig. 15.** Comparison of turbidity and tracer profiles for stations along the ridge (LADDER 2). (a) 9°35'N (cast 6); (b) 9°50'N (cast 9); (c) 9°54'N (cast 100); (d) 10°N (cast 33). The star along the abscissa in (b) is the concentration measured in the AST by *Alvin* on the same day (the *Alvin* sample for (c) gave 0.33 fM, not shown). Unstable portions of the profiles are marked with bold markers. The approximate distances to known vents from the position of the CTD at the bottom of the cast are as follows: (a) 2.5 km; (b) 25 m; (c) 240 m; (d) no known vents in the area.

recorded by LADCP measurements obtained during LADDER 1, and by moored-velocity-profiler data. This flow pattern is also indicated by a 2-D model of the circulation developed by W. Lavelle (McGillicuddy et al., submitted), and such a flow, plus anticyclonic circulation around the seamounts, is indicated by a 3-D model of the circulation in the area, with realistic topography (W. Lavelle, personal communication). The progressive vector diagram from the BMADCP suggests a flow directly to the northwest, rather than north then west (Fig. 5), but, as noted earlier, the LADDER current meter array shows that currents to the west of the ridge were much weaker than those at the

BMADCP. Given the scenario of flow to the north along the western flank of the ridge, it seems very likely that tracer found during the first sampling phase in the AST at 9°50'N was supplied from the patch just to the west of the ridge by local cross-ridge currents (Fig. 6a).

## 6.2. Entrainment of tracer into hydrothermal vent plumes

Vent plumes appear to have entrained on the order of 10% of the injected tracer, with K-vent, in the 9°30'N area, playing the

primary role (Section 5). In the absence of any north-south advection of the initial tracer patch within the AST, the length of the along-AST entrainment zone around K-vent needed to achieve this export is on the order of 120 m. Advection of fluid along the trough could decrease the required size of the entrainment zone by bringing tracer to the latitude of K-Vent. As noted in Section 2.4, the flow at the level of the ridge crest in the 36 h after injection was primarily zonal, i.e., cross-ridge, but with a meridional component, first to the south and then to the north. Deeper in the trough, the meridional component may have predominated due to blocking of the zonal component by the walls of the trough. In addition, the distributed nature of K-vent increases its source area and thus increases its entrainment capability (Lavelle and Wetzler, 1999). It is also possible that undocumented vents in the area may have contributed to the tracer found at the level of vent plumes. In fact, we found a 16 m tall black smoker 600 m south of the injection track (Fig. 4a) during the injection dive. The plume from this vent, which we named PBR-600, may have entrained some tracer.

Both buoyant and non-buoyant near-field vent plumes observed during LADDER 2 far from the injection site were often relatively high in tracer concentration, providing direct evidence of tracer entrainment (see Section 5.3). There were three occasions on which *Alvin* samples were obtained within a day of nearby CTD casts measuring turbidity and tracer in these plumes. The tracer concentrations in the plume in cast 9 were 8 times greater than in the nearby *Alvin* sample (Figs. 8c and 15b), while those in the plumes in cast 91 (profile not shown) and cast 100 (Figs. 8d and 15c) were about half as great as in nearby *Alvin* samples. These observations may seem difficult to reconcile with simple plume models, which predict that AST water entrained into the plumes is diluted by a factor of 100 or so once the plume has reached its level of neutral buoyancy (e.g. Kim et al., 1994, who used the model of Morton et al., 1956). Part of the apparent discrepancy may be due to temporal variability of tracer concentration near the seabed (Fig. 8). Intrinsic temporal variability of buoyant plumes (e.g. Papantoniou and List, 1989) is expected to play a role as well. There is also an ample supply of tracer to be entrained from isopycnal layers well above the AST, where dilution ratios in the plume will be much less, as shown for the overall tracer distribution in Fig. 13 and for particular sites along the ridge crest in Figs. 15b and d.

### 6.3. Implications for larval dispersion

#### 6.3.1. Lateral transport

Identifying the dispersal pathways of larvae from hydrothermal vent fauna is a primary objective of LADDER. A recent eruption along the EPR crest at 9°50'N in late 2005 or early 2006 (Cowen et al., 2007; Tolstoy et al., 2006) left the ridge covered with fresh basalt and devastated the 15-year-old vent communities. A rapid recolonization of the vents in the same area following the 1991 eruption (Shank et al., 1998) raised a number of questions about the source of larvae repopulating the vent communities. Successful recolonization of vents at 9°50'N following eruptions may be due, in part, to vent communities far away supplying larvae.

A passive tracer will behave similarly to neutrally buoyant larvae with little ability to swim against local currents or adjust their buoyancy, conditions that are reasonably assumed for some vent species (Mullineaux and France, 1995). The tracer experiment shows that a vent community at 9°30'N can act as a source population of larvae for colonization of vents along the ridge near 9°50'N, probably via a northward flow along the western flank of the ridge. Furthermore, our results indicate that larvae carried

more than 40 km off-axis may return to the ridge in large quantities within a larval lifetime through reversal of the subinertial regional flows. Adams (2007) hypothesized that such flow reversals at the ridge depth may be due to the passage of mesoscale eddies over the site.

#### 6.3.2. Sheltering

In Section 3.3 we noted that tracer concentrations were often higher in the AST, far from the injection area, than above it. The same seemed to be true of an off-axis depression east of the AST. These observations suggest that larvae may be somewhat sheltered from cross-axis flows in the AST and in similar off-axis depressions. In fact, like the tracer, larval concentrations have been found to be higher in the trough than out of the trough (Mullineaux et al., 2005). Larval retention in the AST would increase the probability of successful colonization. Retention in depressions to the side of the AST would also increase this probability, by slowing dispersion away from the ridge.

#### 6.3.3. The effect of plumes

Our experiment suggests that on the order of 10% of larvae released within 600 m of K-vent can be entrained into its plume. In contrast, Kim and Mullineaux (1998) estimated that only about 3% of larvae spawned within 7 m of a moderate black smoker would be entrained into the hydrothermal plume in the presence of a cross-flow. The higher entrainment rates observed for the tracer may result from several factors. First, it may be due to the large source area (5–10 m<sup>2</sup>) for K-vent mentioned earlier. Lavelle and Wetzler (1999), using the model of Morton et al. (1956), showed that entrainment increases with source area, while Kim and Mullineaux used a model with infinitesimally small source area. Second, the retention capability of the AST coupled with the along-axis component of the currents within the AST following the injection may have kept the tracer in contact with K-vent longer than predicted by a model of a plume in a cross-flow, and, as mentioned above, a cross flow to the west would bring tracer toward K-vent, for a while at least (an hour or so for currents of a few cm/s). Finally, as mentioned above, we cannot rule out the role of vents other than K-vent, both diffuse and discrete, in the entrainment of tracer near 9°30'N.

## 7. Summary

About 3% of the tracer released in the AST at 9°30'N was found in a patch near the vent-rich site at 9°50'N, 36 km to the north, after approximately 40 days. Some of this tracer was found in the axial summit trough around the vents, clearly demonstrating that plankton can be transported from one vent site to another over this distance within the lifetime of important vent larvae. The path taken by this tracer, and particularly the role played by the Lamont Seamounts, is not clear from the tracer data alone, but current meter measurements and numerical models of the circulation indicate the importance of northward flow along the western flank of the ridge (McGillicuddy et al., submitted).

Most of the remainder of the tracer found was displaced off the ridge to the northwest, but was headed back toward the ridge late in the experiment following a reversal of the subinertial currents. This observation illustrates a second pathway from the 9°30'N site to the 9°50'N site resulting from variations in mesoscale currents, perhaps associated with eddies as suggested by Adams (2007).

The tracer was injected along a segment of the AST which included some diffuse sources and, off to the side, K-vent, a moderate-temperature discrete vent surrounded by diffuse sources. Evidence is strong that on the order of 10% of the tracer was entrained into the plume of K-vent, and possibly other nearby

vents, immediately following the injection. This result suggests that a substantial fraction of diffuse source effluent and vent larvae residing within the AST can, in some circumstances, be entrained into the plumes of nearby discrete vents.

### Acknowledgements

This study was funded by NSF Grant OCE-0424953. We wish to thank the LADDER lead investigator L. Mullineaux, and investigators D. McGillicuddy and W. Lavelle for their input and support. We thank B. Guest, C. Sellers, L. Houghton, for their participation in the planning, preparation, and execution of the tracer release experiment. We thank the science parties on the LADDER 1 and 2 cruises, especially S. Beaulieu, I. Garcia-Berdeal, T. Fischer, S. Bennett, N. Kelly, S. Mills, T. Eldson, N. Le Bris, F. Pradillon, L. Corbari, S. Katz, S. Gollner, A. Jackson, and K. Krumhansl, and the crew of DSV *Alvin* and R/V *Atlantis* for their help in the experiment. We also thank the anonymous reviewers whose comments have significantly improved this paper.

### Appendix A. Estimation of the initial tracer plume

Immediately following the injection, the tracer experienced artificial mixing from three sources: the excess density of the tracer, the thermal plume from *Alvin*, and most importantly, the turbulent wake from *Alvin*. Here we estimate the effect of these mixing sources on the spatial extent of the tracer plume shortly after injection.

#### A.1. Displacement due to the density anomaly of the tracer plume

Following theory for buoyant jets and plumes (Fischer et al., 1979), we find that the tracer would have ceased to act as a buoyant jet and displayed characteristics of a buoyant plume 35–40 cm from the injection nozzle, in agreement with visual observations during the injection. To estimate an upper bound for the gravitational descent of the initial plume we twice integrated the reduced gravity estimated from the tracer concentration at this point, about 170 g/m<sup>3</sup>, yielding a vertical distance of 2.4 m by the time the tracer reached the tail of the submersible. Dilution of the plume during its transit along the submersible would reduce the density anomaly of the plume and thus reduce this displacement. Even at this limiting displacement, however, the tracer would still be entrained into *Alvin*'s turbulent wake.

#### A.2. Thermal plume of the submersible

A positively buoyant thermal plume rises from *Alvin* due to the total heat given off by the submersible and its occupants, about 4 kW (personal communication, *Alvin* group). We estimate an upper limit of 12 m for the rise height of the thermal plume, assuming that all of this thermal flux was concentrated in a point source, and using theory for buoyant plumes in a cross flow (Hanna et al., 1982; Middleton, 1986; Lavelle, 1997). The thermal plume is estimated to have ascended between 0.1 and 0.34 m during the passage of the submersible. Interaction of the plume with the submersible, and distribution of the thermal flux over various regions of the submarine rather than at a point, would act to reduce plume rise compared to the above estimates (McDuff, 1995). In any case, the ascent rate of the thermal plume and any tracer it may have entrained would have been slow enough that the plume would have been entrained into the turbulent wake of the submersible.

#### A.3. Turbulent wake of the submersible

The dimensions of the turbulent wake and the associated mixing were estimated using empirical relationships developed for turbulent wakes behind self-propelled bodies in stratified flows. We modeled *Alvin* as a self-propelled cylinder 3 m in diameter and 7 m in length and used the known speed and background stratification to scale the vertical and horizontal dimensions of the turbulent wake in both the near and far field using the empirical equations of Merritt (1974). *Alvin*'s wake would have reached a maximum vertical extent of approximately 14 m before the background stratification inhibited further growth, i.e., within an hour or so. At this point the width of the plume would have been of the same order as the height, but any collapse of the wake and ambient flows in the AST would work to spread the plume across the AST. In fact, relationships developed for horizontal spreading of diffuse source plumes (Trivett, 1994) suggest the tracer plume would have mixed across the AST within an hour or so just by ambient flows in the AST. We conclude that the tracer plume was fairly well dispersed within the AST along the injection reach within an hour of the passage of the submersible.

### References

- Adams, D.K., 2007. Influence of hydrodynamics on the larval supply to hydrothermal vents on the east Pacific Rise. Sc. D. thesis, MIT/WHOI Joint Program, Massachusetts Institute of Technology/Woods Hole Oceanographic Institution, Woods Hole, MA.
- Adams, D.K., Mullineaux, L.S., 2008. Supply of gastropod larvae to hydrothermal vents reflects transport from local larval sources. *Limnology and Oceanography* 53 (5), 1945–1955.
- Baker, E.T., Massoth, G.J., Walker, S.L., Embley, R.W., 1993. A method for quantitatively estimating diffuse and discrete hydrothermal discharge. *Earth and Planetary Science Letters* 118, 235–249.
- Baker, E.T., Feely, R.A., Mottl, M.J., Sansone, F.T., Wheat, C.G., Resing, J.A., Lupton, J.E., 1994. Hydrothermal plumes along the East Pacific Rise, 8°40' to 11°50'N: 1 plume distribution and relationship to the apparent magmatic budget. *Earth and Planetary Science Letters* 128, 1–17.
- Chevaldonné, P., Jollivet, D., Vangriesheim, A., Desbruyères, D., 1997. Hydrothermal-vent alvinellid polychaete dispersal in the eastern Pacific: 1 influence of vent site distribution, bottom currents, and biological patterns. *Limnology and Oceanography* 42, 67–80.
- Cowen, J.P., et al., 2007. Volcanic eruptions at East Pacific Rise near 9°50'N. *Eos, Transactions of the American Geophysical Union* 88 (7), 81.
- Craig, H., 1990. The Helios helium-3 section: implications for the deep water circulation in the North and South Pacific. *Eos, Transactions of the American Geophysical Union* 71 (28), 882.
- Fischer, H.B., List, E.J., Koh, R.C.Y., Imberger, J., Brooks, N.H., 1979. Mixing in Inland and Coastal Waters. Academic Press, New York, p. 483.
- Fornari, D.J., Haymon, R.M., Perfit, M.R., Gregg, T.K.P., Edwards, M.H., 1998. Axial summit trough of the East Pacific Rise 9–10°N: geological characteristics and evolution of the axial zone on fast spreading mid-ocean ridges. *Journal of Geophysical Research* 103 (B5), 9827–9855.
- Hanna, S.R., Briggs, G.A., Hosker Jr., R.P., 1982. Handbook of Atmospheric Diffusion. Technical Information Center, U. S. Department of Energy, Washington D.C. 102 pp.
- Kim, S.T., Mullineaux, L.S., 1998. Distribution and near-bottom transport of larvae and other plankton at hydrothermal vents. *Deep-Sea Research II* 45, 423–440.
- Kim, S.L., Mullineaux, L.S., Helfrich, K.R., 1994. Larval dispersal via entrainment into hydrothermal vent plumes. *Journal of Geophysical Research* 99, 12,655–12,665.
- Law, C.S., Watson, A.J., Liddicoat, M.I., 1994. Automated vacuum analysis of sulphur hexafluoride in seawater: derivation of the atmospheric trend (1970–1993) and potential as a transient tracer. *Marine Chemistry* 48, 57–69.
- Lavelle, J.W., 1997. Buoyancy-driven plumes in rotating, stratified cross flows: plume dependence on rotation, turbulent mixing, and cross-flow strength. *Journal of Geophysical Research* 102, 3405–3420.
- Lavelle, J.W., Wetzler, M.A., 1999. Diffuse venting and background contributions to chemical anomalies in a neutrally buoyant ocean hydrothermal plume. *Journal of Geophysical Research* 104, 3201–3209.
- Lavelle, J.W., Wetzler, M.A., Embley, R.W., 2001. Prospecting for hydrothermal vents using moored current and temperature data: Axial Volcano on the Juan de Fuca Ridge, Northeast Pacific. *Journal of Physical Oceanography* 31, 827–838.
- Lupton, J.E., 1998. Hydrothermal helium plumes in the Pacific Ocean. *Journal of Geophysical Research* 103 (C8), 15,853–15,868.

- Marsh, A.G., Mullineaux, L.S., Young, C.M., Manahan, D.T., 2001. Larval dispersal potential of the tubeworm *Riftia pachyptila* at deep-sea hydrothermal vents. *Nature* 411, 77–80.
- Macdonald, K.C., Fox, P.J., Miller, S., Carbotte, S., Edwards, M.H., Elsen, M., Fornari, D.J., Perram, L., Pockalny, R., Scheirer, D., Tighe, S., Welland, C., Wilson, D., 1992. The East Pacific Rise and its flanks 8–18 N: history of segmentation, propagation and spreading direction based on Sea-MARC II and Sea Beam studies. *Marine Geophysical Researches* 14, 299–344.
- McDuff, R.E., 1995. Physical dynamics of deep-sea hydrothermal systems. In: Humphris, S.E., Zierenberg, R.A., Mullineaux, L.S., Thomson, R.E. (Eds.), *Seafloor hydrothermal systems: physical, chemical, biological, and geochemical interactions*. American Geophysical Union, Washington D.C, pp. 357–368.
- McGillicuddy Jr., D.J., Lavelle, J.W., Mullineaux, L.S., Thurnherr, A.M., Kosneyrev, V.K., Larval dispersion along an axially symmetric mid-ocean ridge. *Deep-Sea Research I*, submitted.
- Merritt, G.E., 1974. Wake growth and collapse in stratified flow. Paper 73–108 American Institute of Aeronautics and Astronautics 11th Aerospace Meeting, Washington, D.C.
- Middleton, J.H., 1986. The rise of forced plumes in a stably stratified crossflow. *Boundary-Layer Meteorology* 36, 187–199.
- Morton, B.R., Taylor, G., Turner, J.S., 1956. Turbulent gravitational convection from maintained and instantaneous sources. *Proceedings of the Royal Society of London, Series A* 234, 1–23.
- Mullineaux, L.S., France, S.C., 1995. Dispersal mechanisms of deep-sea hydrothermal vent fauna. *American Geophysical Union Geophysical Monograph* 91, 408–424.
- Mullineaux, L.S., Mills, S.W., Sweetman, A.K., Beaudreau, A.H., Metaxas, A., Hunt, H.L., 2005. Vertical, lateral, and temporal structure in larval distribution at hydrothermal vents. *Marine Ecology Progress Series* 293, 1–16.
- Mullineaux, L.S., Speer, K.G., Thurnherr, A.M., Maltrud, M.E., Vangriesheim, A., 2002. Implications of cross-axis flow for larval dispersal along mid-ocean ridges. *Cahiers de Biologie Marine* 43, 281–284.
- Papantoniou, D., List, E.J., 1989. Large-scale structure in the far field of buoyant jets. *Journal of Fluid Mechanics* 209, 151–190.
- Rona, P.A., Trivett, D.A., 1992. Discrete and diffuse heat transfer at ASHES vent field, Axial Volcano, Juan de Fuca Ridge. *Earth and Planetary Science Letters* 109, 57–71.
- Sempere, J.C., Macdonald, K.C., 1986. Deep-tow studies of the overlapping spreading centers at 9°03'N on the East Pacific Rise. *Tectonics* 5, 881–900.
- Shank, T.M., Fornari, D.J., Von Damm, K.L., Lilley, M.D., Haymon, R.M., Lutz, R.A., 1998. Temporal and spatial patterns of biological community development at nascent deep-sea hydrothermal vents (9°50'N, East Pacific Rise). *Deep-Sea Research* 45, 465–515.
- Smith, W.H.F., Sandwell, D.T., 1997. Global sea floor topography from satellite altimetry and ship depth soundings. *Science* 277, 1956–1962.
- Sortland, L.D., Robinson, D.B., 1964. The hydrates of methane and sulphur hexafluoride. *Canadian Journal of Chemical Engineering* 42, 38–42.
- Talley, L.D., Johnson, G.C., 1994. Deep, zonal subequatorial currents. *Science* 263, 1125–1128.
- Thurnherr, A.M., Richards, K.J., 2001. Hydrography and high-temperature heat flux of the Rainbow hydrothermal site (36°14'N, Mid-Atlantic Ridge). *Journal of Geophysical Research* 106, 9411–9426.
- Tolstoy, M., Cowen, J.P., Baker, E.T., Fornari, D.J., Rubin, K.H., Shank, T.M., Waldauser, F., Bohnenstiehl, D.R., Forsyth, D.W., Holmes, R.C., Love, B., Perfit, M.R., Weekly, R.T., Soule, S.A., Glazer, B., 2006. A sea-floor spreading event captured by seismometers. *Science* 314, 1920–1922.
- Trivett, D.A., 1994. Effluent from diffuse hydrothermal venting 1. A simple model of plumes from diffuse hydrothermal sources. *Journal of Geophysical Research* 99, 18,403–18,415.
- Watson, A.J., Liddicoat, M.I., Ledwell, J.R., 1987. Perfluorodecalin and sulphur hexafluoride as purposeful marine tracers: some deployment and analysis techniques. *Deep-Sea Research* 34, 19–31.
- Watson, A.J., Ledwell, J.R., 2000. Oceanographic tracer release experiments using sulphur hexafluoride. *Journal of Geophysical Research* 105, 14,325–14,337.
- White, S.M., Haymon, R.M., Carbotte, S., 2006. A new view of ridge segmentation and near-axis volcanism at the East Pacific Rise, from EM300 multibeam bathymetry. *Geochemistry Geophysics Geosystems* 7, Q1205, doi:10.1029/2006GC001407.